Tuning characteristics of a metamaterial beam with lateral-electric-field piezoelectric shuntings

Tingfeng Ma [a],[*], Yangyang Chen [b], Hui Chen [b], Yuanzhen Zheng [a], Guoliang Huang [b],[**], Ji Wang [a], Jianke Du [a]

[a] School of Mechanical Engineering and Mechanics, Ningbo University, Ningbo 315211, China
[b] Department of Mechanical and Aerospace Engineering, University of Missouri, Columbia, Missouri 65211, USA

ARTICLE INFO

ABSTRACT

Metamaterials with piezoelectric shuntings have convenient tunability. The increase in the resistance value in the shunting circuit can broaden the bandgap width but lower the vibration attenuation ability. In this study, a piezoelectric unit cell with a lateral electric field (LEF) is applied to a metamaterial beam to improve the resistance-tuning characteristics. The effective stiffness and bandgaps were calculated by using a theoretical method and verified by three-dimensional numerical simulations. Compared with resonators with a thickness electric field, LEF resonators have a stronger piezoelectric coupling, and the extra transferred energy of LEF resonators is reflected in the greater vibration attenuation depth when the increasing degrees of the bandgap widths of the two cases are similar. Therefore, the LEF metamaterial beam exhibits better resistance-tuning characteristics; namely, it can maintain better vibration attenuation properties when the bandgap width is broadened by increasing the resistance value.

1. Introduction

Acoustic metamaterials are composite structures that exhibit unusual effective physical properties that do not exist in natural materials. Acoustic metamaterials can be designed to tailor elastic wave dispersion by using Bragg scattering or local resonances. For Bragg scattering [1–4], the wavelength is on the order of the lattice constants in the propagation direction; consequently, low-frequency Bragg-type bandgaps require large structure sizes. For locally resonant acoustic metamaterials [5–8], bandgaps at wavelengths over two orders of magnitude longer than the lattice size can be realized, providing a medium with unusual mechanical properties at long wavelengths.

Huang et al. showed that, for an acoustic metamaterial with mass-in-mass unit cells, the effective mass density can be negative near the resonance frequency [9]. Nouh et al. experimentally realized acoustic metamaterials using beams and plates and verified the bandgap and vibration attenuation ability of metamaterials [10]. Raghavan et al. [11] developed a receptance coupling technique for analyzing flexural wave transmission in a periodic structure and found that stronger inertia of the resonator could increase the local resonance bandgap width. In addition, for acoustic metamaterials with local resonances, sound isolation and vibration suppression [12–15] were explored by using the acoustic and vibration attenuation characteristics of bandgaps.

---

* Corresponding author: Tingfeng Ma, School of Mechanical Engineering and Mechanics, Ningbo University, Ningbo 315211, China
** Corresponding author: Guoliang Huang, Department of Mechanical and Aerospace Engineering, University of Missouri, Columbia, Missouri 65211, USA
E-mail addresses: matingfeng@nbu.edu.cn (T. Ma), huangg@missouri.edu (G. Huang).

For the above metamaterials with mechanical local resonances, tuning the material performances usually requires modifications of physical structure parameters, which is extremely inconvenient for their application in practical engineering. For a metamaterial combined with smart materials and the corresponding electric circuits, the effective material properties can be tuned electrically without changing the structure parameters. Piezoelectric materials play an important role in tuning and controlling the elastic and acoustic properties of metamaterials. Hagood and von Flotow presented the first theoretical formulation for piezoelectric shuntings [16]. Based on this, some piezoelectric shunting designs have been presented to improve the acoustic and vibration performances of dynamic structures [17–23]. In addition, several other important results in this field have been achieved in recent years. Zhou et al. found that the enhanced metadamping phenomenon could emerge by using a negative-capacitance-enhanced resonant shunt on band structures [24]. Jin et al. [25] proposed a resonant structure of a hard core coated by piezoelectric composite materials as an acoustic metamaterial, in which a negative effective mass density and elastic modulus are simultaneously achieved and the bandwidth is sensitive to the piezoelectric constant e_{33}. Chen et al. presented a tunable acoustic metamaterial with double negativity composed of side holes and periodic membranes, the tension and stiffness of which are actively controlled by electromagnets producing additional stresses [26]. In addition, Airoldi and Ruzzene controlled wave attenuation by placing periodic shunted piezoelectric patches with resistance–inductance circuits along the beam [27].

For traditional piezoelectric metamaterials, the bandgap width can be increased to some extent by tuning the resistance value in the shunt circuit. However, the vibration attenuation capability decreases considerably [28]. The vibration attenuation capability is closely related to the strength of piezoelectric coupling of the piezoelectric resonators. For typical piezoelectric resonators with a thickness electric field (TEF), the effective piezoelectric coupling coefficient is k_{31}, which is proportional to the piezoelectric constant d_{31}. For typical piezoelectric resonators with a lateral electric field (LEF), k_{33} is the effective piezoelectric coupling coefficient, which is proportional to the piezoelectric constant d_{33}. In [29], to realize a unimorph piezoelectric actuator using the piezoelectric constant d_{33}, a caterpillar-type piezoelectric transducer was bonded to a metal plate along the polarization direction (d_{33}) and was shown to exhibit good actuating effectiveness. Piezoelectric materials used for resonators in metamaterials mainly focus on piezoelectric materials from the lead-zirconate-titanate (PZT) class because of their good dielectric, ferroelectric, piezoelectric, and mechanical properties. For widely used PZT-class piezoelectric materials, d_{33} is much higher than d_{31} [30]. For example, for PZT-5H, d_{33} is twice as high as d_{31}. Therefore, for widely used PZT-class piezoelectric materials, LEF devices have stronger piezoelectric coupling compared to TEF devices. LEF metamaterials are thus expected to have better vibration attenuation capability when the resistance value is tuned for a wider bandgap. This work focuses on piezoelectric metamaterial beams based on the LEF. A piezoelectric unit cell with an LEF resonator is proposed to improve the resistance-tuning characteristics of metamaterial beams. The effective stiffness and bandgaps were determined theoretically, and three-dimensional numerical simulations were employed to verify the theoretical results.

2. Theory

The dynamic behaviors of a locally resonant piezoelectric metamaterial beam with an LEF are considered in this study. The locally resonant metamaterial beam includes a host beam and a periodic array of shunted piezoelectric transducers, as shown in Fig. 1(a). Fig. 1(b) shows the traditional piezoelectric unit cell with a TEF, where the z axis is along the direction of the thickness of the piezoelectric patch. Fig. 1(c) shows the piezoelectric unit cell with an LEF, where the z axis is normal to the direction of the thickness of the piezoelectric patch.

In this work, the crystal for the LEF configuration is polarized along the length direction, and the crystal for the TEF configuration is polarized along the thickness direction. Along the width direction, vibrations in the length direction are uniform. For the unit cell with a TEF, the effective piezoelectric constant is d_{31}, whereas that for the unit cell with an LEF is d_{33}. In this section, Euler–Bernoulli theory is used to analyze the dynamic behaviors of the metamaterial beam, which behaves as a one-dimensional waveguide that supports the propagation of axial and transverse waves. Based on force and moment balances, the transverse, $w(z, t)$, and axial, $u(z, t)$, motions of the beam shown in Fig. 1 can be described by the following differential equations:

$$\frac{\partial^2}{\partial z^2}\left[D(z)\frac{\partial^2}{\partial z^2}w(z,t)\right] + m(z)\frac{\partial^2}{\partial t^2}w(z,t) = 0,$$

$$\frac{\partial^2}{\partial z^2}\left[E(z)\frac{\partial}{\partial z}u(z,t)\right] - m(z)\frac{\partial^2}{\partial t^2}u(z,t) = 0,$$

(1)

$$\frac{\partial^2}{\partial x^2}\left[D(z)\frac{\partial^2}{\partial z^2}w(z,t)\right] - B(z)\frac{\partial^3}{\partial z^3}u(z,t) + m(z)\frac{\partial^2}{\partial t^2}w(z,t) = 0,$$

$$\frac{\partial^2}{\partial x^2}\left[E(z)\frac{\partial}{\partial z}u(z,t)\right] - B(z)\frac{\partial^3}{\partial z^3}w(z,t) - m(z)\frac{\partial^2}{\partial t^2}u(z,t) = 0,$$
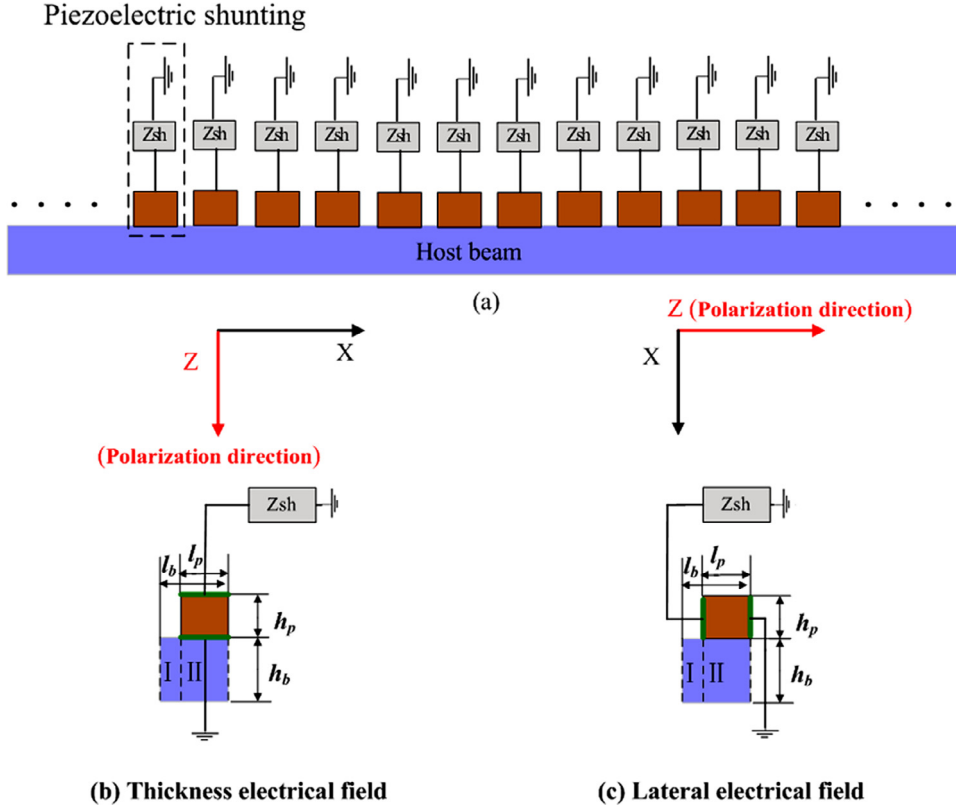
(2)

Fig. 1. (a) Metamaterial beam with an array of shunted piezoelectric patches. (b) Unit cell with a TEF. (c) Unit cell with an LEF.

where $D(z)$ and $E(z)$ denote the bending stiffness and axial stiffness of the beam, respectively, $B(z)$ is the coupling item, and $m(z)$ is the mass per unit area. The four items given above can be expressed as follows:

$$m(z)=\begin{cases} \rho_b A_b, -(l_b-l_p)<z\leq 0, \\ \rho_b A_b+\rho_p A_p, 0<z\leq l_p, \end{cases}$$ (3)

$$E(z)=\begin{cases} E_b A_b, -(l_b-l_p)<z\leq 0, \\ E_b A_b+E_p^{su}(\omega)A_p, 0<z\leq l_p, \end{cases}$$ (4)

$$B(z) = \begin{cases} 0, -(l_b-l_p)<z\leq 0, \\ \frac{-E_b b_b h_b h_p 3}{2}+E_p^{su}(\omega)b_p\left(\frac{h_p^3}{12}+\frac{h_b+h_p 2}{4}\right), 0<z\leq l_p, \end{cases}$$ (5)

$$D(z)=\begin{cases} \frac{E_b b_b h_b^3}{12}, -(l_b-l_p)<z\leq 0, \\ \frac{E_b b_b h_b^3}{12}+\frac{E_p^{su}(\omega)b_p\left[(h_b+h_p)^3-h_b^3\right]}{12}, 0<z\leq l_p, \end{cases}$$ (6)

where α denotes the ratio between the length of the interval with no piezoelectric patch $(l_b - l_p)$ and the length of the period (l_b); h_b and h_p are the thicknesses of the host beam and piezoelectric patch, respectively; ρ_b and ρ_p are the densities of the host beam material and the piezoelectric material, respectively; and b_b and b_p are the widths of the host beam and piezoelectric patch, respectively. In addition, $A_b=h_b b_b$ and $A_p=h_p b_p$. Young's modulus of the shunted patch can be obtained by using Hagood's [16] method with the following expression:

$$E_p^{su}(\omega)=E_p^D\left(1 - \frac{k_{33}^2}{1 + i\omega C_p^\varepsilon Z^{SU}(\omega)}\right),$$ (7)

where ω is the frequency, E_p^D is Young's modulus of the piezoelectric material when the shunting circuit is open, $Z^{SU}(\omega)$ is the electrical impedance of the shunting circuit, C_p^ε is the capacitance of the piezoelectric transducer at constant strain, and k_{33} is the piezoelectric coupling coefficient for the unit cell with an LEF.

In our case, for the LEF metamaterials, the aluminum beam and the piezoelectric plate are bonded together through an electrically insulated bonding layer, similar to the unimorph piezoelectric actuator using piezoelectric constant d_{33} [29].

This can prevent electron transfer from the piezoelectric plate to the metal plate. Therefore, energy transfer between the piezoelectric plate and the aluminum beam is only embodied in mechanical items.

The coupled system of Eqs. (1) and (2) can be written in matrix form as

$$\mathbf{A}(z)\frac{d}{dx}\mathbf{F}(z)=\mathbf{L}(z)\mathbf{F}(z), \tag{8}$$

where $\mathbf{A}(z)$ and $\mathbf{L}(z)$ are two coefficient matrices and the state vector $\mathbf{F}(x)$ is defined as

$$\mathbf{F}(z) = [u, w, w, z, N, M, Q]^{T}, \tag{9}$$

where N,M, and Q are the axis stress resultant, bending moment, and shear force, respectively.

The matrices $\mathbf{A}$ in Eq. (8) are defined as follows: for Region I,

$$\mathbf{A}(z)=\begin{bmatrix} E(z) & 0 & 0 & 0 & 0 & 0 \\ 0 & 1 & 0 & 0 & 0 & 0 \\ 0 & 0 & D(z) & 0 & 0 & 0 \\ 0 & 0 & 0 & 1 & 0 & 0 \\ 0 & 0 & 0 & 0 & -1 & 0 \\ 0 & 0 & 0 & 0 & 0 & 1 \end{bmatrix}; \tag{10}$$

for Region II,

$$\mathbf{A}(z)=\begin{bmatrix} E(z) & 0 & -B(z) & 0 & 0 & 0 \\ 0 & 1 & 0 & 0 & 0 & 0 \\ B(z) & 0 & D(z) & 0 & 0 & 0 \\ 0 & 0 & 0 & 1 & 0 & 0 \\ 0 & 0 & 0 & 0 & -1 & 0 \\ 0 & 0 & 0 & 0 & 0 & 1 \end{bmatrix}. \tag{11}$$

The matrices $\mathbf{L}$ in Eq. (8) are defined as follows:

$$\mathbf{L}(z)=\begin{bmatrix} 0 & 0 & 0 & 1 & 0 & 0 \\ 0 & 0 & 1 & 0 & 0 & 0 \\ 0 & 0 & 0 & 0 & 1 & 0 \\ -\omega^2 m(z) & 0 & 0 & 0 & 0 & 0 \\ 0 & 0 & 0 & 0 & 0 & 1 \\ 0 & -\omega^2 m(z) & 0 & 0 & 0 & 0 \end{bmatrix}. \tag{12}$$

Eq. (8) can be rewritten as

$$\frac{d}{dz}\mathbf{F}(z)=\mathbf{J}(z)\mathbf{F}(z), \tag{13}$$

$$\mathbf{J}(z) = \mathbf{A}^{-1}(z)\mathbf{L}(z). \tag{14}$$

$z = -\alpha l_b$Based on the expression for the analytical solution of Eq. (13), the relationship between the physical quantities for and $z = 0$ in the unit cell shown in Fig. 1(c) can be obtained as

$$\mathbf{F}(0) = e^{\alpha l_b \mathbf{J_1}}\mathbf{F}(-\alpha l_b), \tag{15}$$

where$\mathbf{J_1}=\mathbf{J}(z), -\alpha l_b < z \leq 0$. The relationship between the physical quantities for $z=0$ and $z = (1 - \alpha)l_b$ is

$$\mathbf{F}[(1 - \alpha)l_b] = e^{(1-\alpha)l_b \mathbf{J_2}}\mathbf{F}(0), \tag{16}$$

$z = -\alpha l_b$where $\mathbf{J_2} = \mathbf{J}(z), 0 < z \leq (1 - \alpha)l_b$.Therefore, the physical quantities between and $z = (1 - \alpha)l_b$ can be related by

$$\mathbf{F}[(1 - \alpha)l_b)]=e^{\alpha l_b \mathbf{J_1}}e^{(1-\alpha)l_b \mathbf{J_2}}\mathbf{F}(-\alpha l_b). \tag{17}$$

According to Bloch's theorem, the wave fields $\mathbf{F}[(1 - \alpha)l_b]$ and $\mathbf{F}(-\alpha l_b)$ are satisfied by

$$\mathbf{F}[(1 - \alpha)l_b]=\lambda\mathbf{F}(-\alpha l_b), \tag{18}$$

where $\lambda = e^{ikl_b}$and k are the wavenumbers.

Comparing Eqs. (17) and (18) reveals that the dispersion relationships can be determined by solving the eigensystem problem given as

$$e^{\alpha l_b \mathbf{J_1}}e^{(1-\alpha)l_b \mathbf{J_2}}\mathbf{F}(-\alpha l_b) = \lambda\mathbf{F}(-\alpha l_b). \tag{19}$$

Table 1
Geometric and material parameters of the shunted piezoelectric beam.

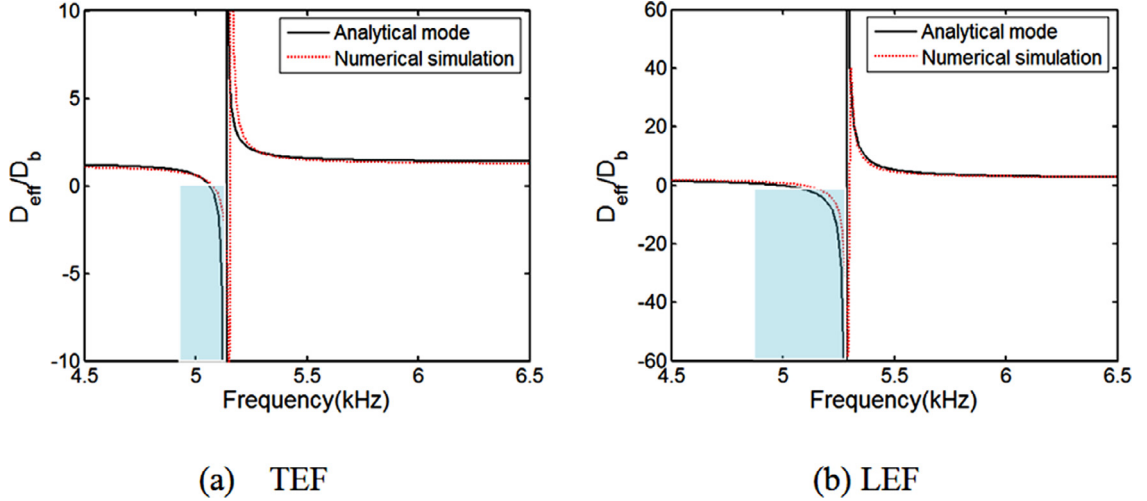| Geometric parameters (mm)							
l_b	3.5	l_p	3.2				
h_b	2.5	h_p	2				
b_b	6.4	b_p	6.4				
Material parameters							
E_b	69 GPa	E_P	63 GPa	ρ_b		2700 g•m^{-3}	
ρ_p	7600 kg•m^{-3}	$C_{11}{}^E$	126 GPa	$C_{12}{}^E$		79.5 GPa	
$C_{13}{}^E$	84.1 GPa	$C_{33}{}^E$	117 GPa	$C_{44}{}^E$		23 GPa	
$C_{66}{}^E$	23.25 GPa	e_{15}	17 C/m^2	e_{31}		-6.55 C/m^2	
e_{33}	23.3 C/m^2	d_{31}	-2.74×10^{-12}	d_{31}		5.93×10^{-12}	
$\varepsilon_{11}{}^S$	1700 ε_0	$\varepsilon_{33}{}^S$	1470ε_0	$\varepsilon_{33}{}^T$		3443ε_0	

Fig. 2. Normalized effective bending stiffnesses for (a) TEF and (b) LEF metamaterial beams.

3. Effective material parameters

For the analysis of specific cases, an inductance element is used as the shunt circuit. It should be noted that a piezo-electric transducer acts as a capacitor. An L-C resonant unit is formed by the combination of the piezoelectric capacitance and inductor shunt. The resonance frequency is determined by $\omega_{LC}^2 = 1/2LC$[16]. The host beam was made of aluminum. The piezoelectric material of the transducer was PZT-5H. The geometric and material parameters of the unit cells are listed in Table 1. For the TEF and LEF unit cells considered in this work, C is 307 and 112 pF, respectively. To obtain a resonance frequency of approximately 5 kHz, L was set to 3300 and 9025 mH for the TEF and LEF unit cells, respectively. The resistance values were both set to zero.

To obtain the effective bending stiffness, the harmonic rotational angles at the left boundary ($z = -\alpha l_b$) and the right boundary ($z = (1 - \alpha)l_b$) of the unit cell were set as ϕ_{-pr} and ϕ_{pr}, respectively. In addition, the transverse displacements at the two boundaries were set to zero. The longitudinal displacement on the left boundary ($z = -\alpha l_b$) of the unit cell was fixed, and the longitudinal force on the right boundary ($z = (1 - \alpha)l_b$) was set to zero, and thus the global reaction bending moments on the boundaries can be obtained naturally with respect to the rotational center. The effective bending stiffness D_{eff} of the metamaterial beam can be obtained using

$$D_{eff} = \frac{M[z = (1 - \alpha)p]}{2\phi_{pr}/l_b},\tag{20}$$

where $M[z = (1 - \alpha)l_b]$ denotes the global reaction bending moment calculated at the right boundary.

The normalized effective bending stiffnesses D_{eff}/D_b, where D_b is the bending stiffness of the host beam, were calculated analytically and verified based on numerical simulations using COMSOL over the frequencies of interest. The geometric and material parameters were set according to Table 1. The geometric and boundary conditions are the same in the analytical model and in the COMSOL simulation. Fig. 2 shows the calculated effective bending stiffness values. Owing to the out-of-phase motions of the resonator and host beam, negative effective bending stiffnesses emerge in the shaded areas, which represent the bandgaps. The analytical results are in good agreement with the numerical simulation results. This verifies the validity of the effective stiffness calculations in the analytical model. Figs. 2(a) and 2(b) show that the bandgap widths for the TEF and LEF metamaterial beams are nearly 0.21 and 0.47 kHz, respectively.
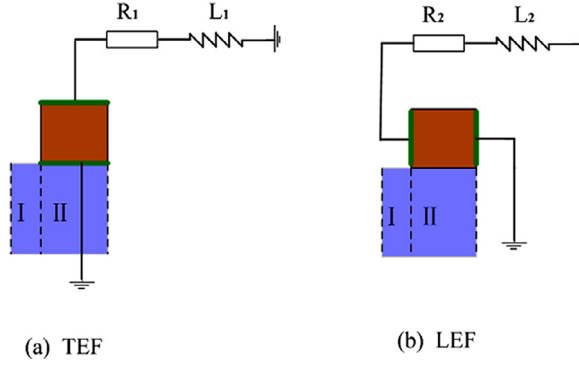
Fig. 3. Unit cells with shunted piezoelectric patches and *R-L* circuits: (a) TEF; (b) LEF.
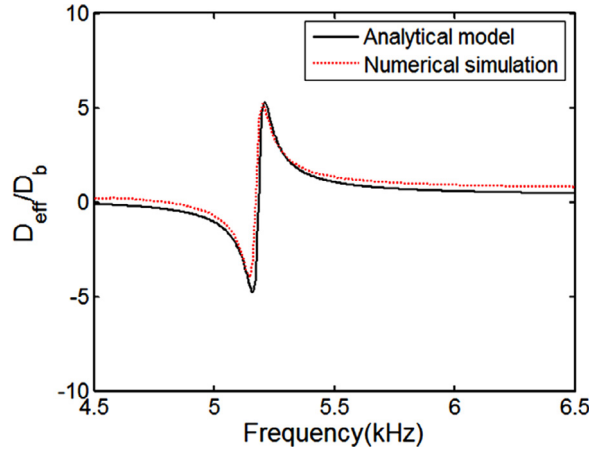

Fig. 4. Normalized effective bending stiffnesses for LEF metamaterial beams with a shunting resistance of 2.8 kΩ and an inductance of 9025 mH.

4. Tuning characteristics

Unit cells with shunted piezoelectric patches and *R-L* circuits were considered in TEF and LEF metamaterial beams, as shown in Fig. 3.

When a large resistor is included in the shunting circuit, the consistency of the effective bending stiffness from the analytical model and numerical simulation was further checked. Fig. 4 shows the normalized effective bending stiffnesses for LEF metamaterial beams with a shunting resistance of 2.8 kΩ and an inductance of 9025 mH. The resonance frequency from the numerical simulation result is 5.196 kHz. According to $f_s = \frac{1}{2\pi\sqrt{L\cdot C}}$, the capacitance of the actuator from the numerical simulation is 106 pF. The results of the resonance frequency and capacitance are close to those from the analytical model, namely, 5.213 kHz and 105.4 pF.

In addition, Fig. 4 shows that the normalized effective bending stiffness values for LEF metamaterial beams obtained by the finite element model approximately agree with the theoretical results when a large resistor is included in the shunting circuit.

The normalized effective bending stiffness D_{eff}/D_b as functions of both the frequency and inductance values are quantitatively illustrated for the TEF and LEF metamaterial beams in Figs. 5(a) and 5(b), respectively. In this case, the resistance values R_1 and R_2 were both set to 100 Ω. It can be seen that, for both the TEF and LEF metamaterial beams, the region of negative normalized effective bending stiffness is primarily sensitive to the inductance value. The tunable frequency bands for bending wave attenuations in the metamaterial beam controlled by different inductances are examined based on the theoretical results of the dispersion curves, which are obtained using Eq. (19). The results are shown in Figs. 5(c) and 5(d), where frequency$_H$ and frequency$_L$ are the high and low boundary frequencies of the bandgap, respectively. The central frequency decreases with increasing inductance; however, the bandgap width is nearly unaffected because the central frequency of the bandgap is primarily determined by the *L-C* resonance frequency. The trends of the bandgaps shown in Figs. 5(c) and 5(d) are in good agreement with those of the normalized effective bending stiffness shown in Figs. 5(a) and 5(b), respectively.

The normalized effective bending stiffness values as functions of both the frequency and resistance values are quantitatively illustrated in Figs. 6(a) and 6(b). To obtain a resonance frequency of approximately 5 kHz, L_1 and L_2 were set to 3300

(a) Normalized effective bending stiffness of TEF   **(b)** Normalized effective bending stiffness of LEF

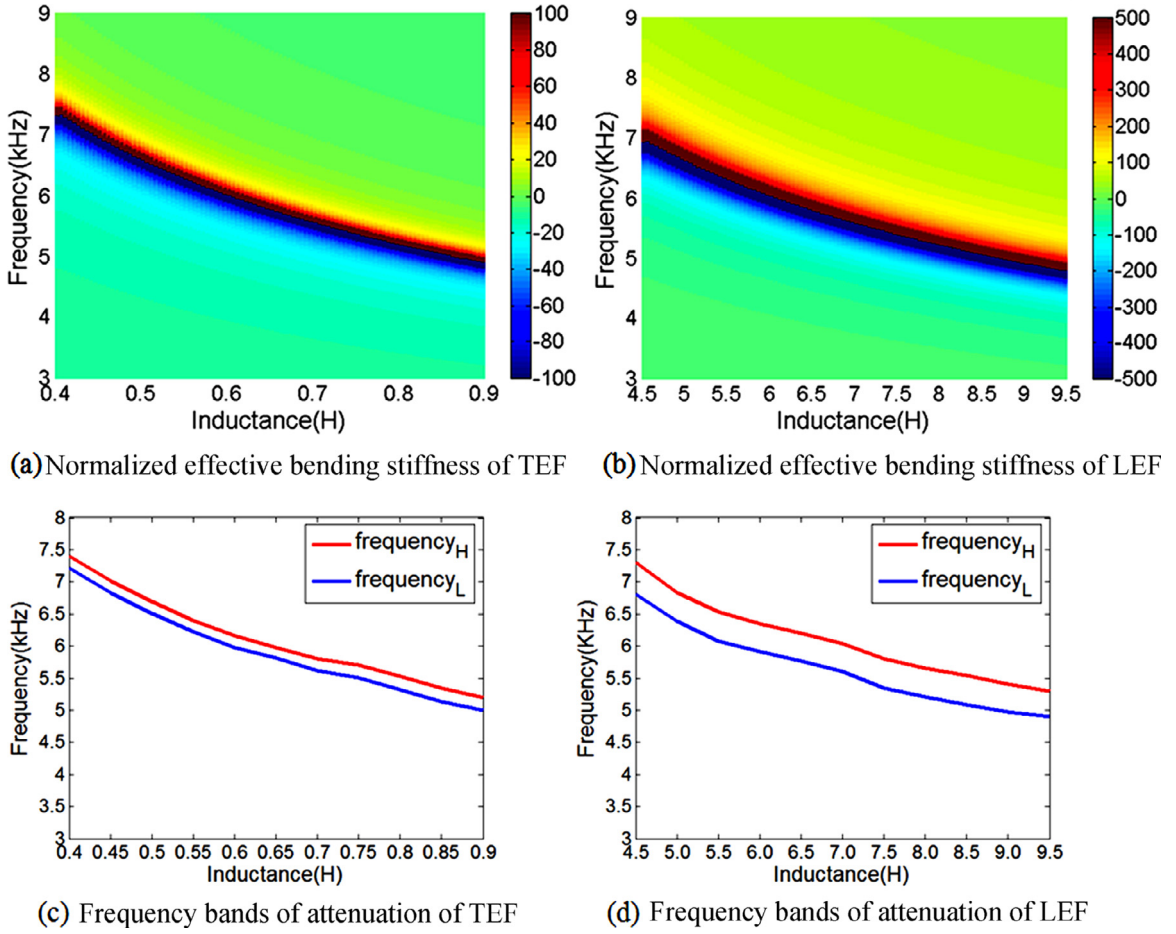**(c)** Frequency bands of attenuation of TEF   **(d)** Frequency bands of attenuation of LEF

Fig. 5. Tuning characteristics of the TEF and LEF metamaterial beams with different inductance values. (a) and (b) Normalized effective bending stiffnesses (D_{eff}/D_b) as functions of both frequency and inductance value for TEF and LEF, respectively, where the unit of the normalized effective bending stiffnesses (D_{eff}/D_b) is 1. (c) and (d) Relationships between the frequency bands for bending wave attenuation and the inductance values based on the theoretical results of dispersion curves obtained by using Eq. (19) for TEF and LEF, respectively; frequency$_H$ and frequency$_L$ denote the high and low boundary frequencies of the bandgap, respectively.

and 9025 mH for the TEF and LEF unit cells, respectively. For both TEF and LEF metamaterial beams, the region of negative normalized effective bending stiffness is primarily influenced by the resistance value. Figs. 6(c) and 6(d) show the relationships between the frequency bands for bending wave attenuation and the resistance values based on the theoretical results of the dispersion curves for the TEF and LEF unit cells, respectively, which are obtained by using Eq. (19). The trends in the normalized effective bending stiffness shown in Figs. 6(a) and 6(b) agree well with those of the bandgaps shown in Figs. 6(c) and 6(d), respectively. As the value of the resistance increases, the bandgap width increases continuously. Electrical damping increases as the resistance value increases, thereby resulting in greater vibration damping as a result of the piezoelectric effect. Namely, the metadamping of the locally resonant metamaterial beam increases as the resistance value increases, thereby leading to a decrease in the quality factor (Q factor) for the resonance, and thus the bandgap width becomes larger. For metamaterials with piezoelectric shuntings, when the resistance value increases, the bandgap will be broadened, but the vibration attenuation ability will be weakened. The aim here is to assess the resistance-tuning characteristic rationally, namely, to compare the decreasing degree of the vibration attenuation ability when the increase extents of the bandgaps of LEF and TEF are the same. Here, the vibration attenuation abilities of TEF and LEF metamaterial beams are compared when the bandgaps increase to two times of those for $R = 0$. For the TEF, when R increased from 0 to 0.8 kΩ, the bandgap doubled, as shown in Fig. 6(c). For the LEF, when R increased from 0 to 20 kΩ, the bandgap doubled, as shown in Fig. 6(d). Therefore, two resistance values were selected to assess the resistance-tuning characteristics of TEF and LEF metamaterials. The transmission curves obtained by COMSOL simulations of the TEF metamaterial beam for $R = 0$ and 0.8 kΩ are shown in Figs. 6(e) and 6(f), respectively. The results show that, as the R value increased from 0 to 0.8 kΩ, the Q factor changed from 128 to 6, and wave attenuation became weaker obviously (the transmission value increased from 0.018 to 0.67). In addition, the transmission curves for $R = 0$ and 20 kΩ are shown for the LEF metamaterial beam in Figs. 6(g) and 6(h), respectively.
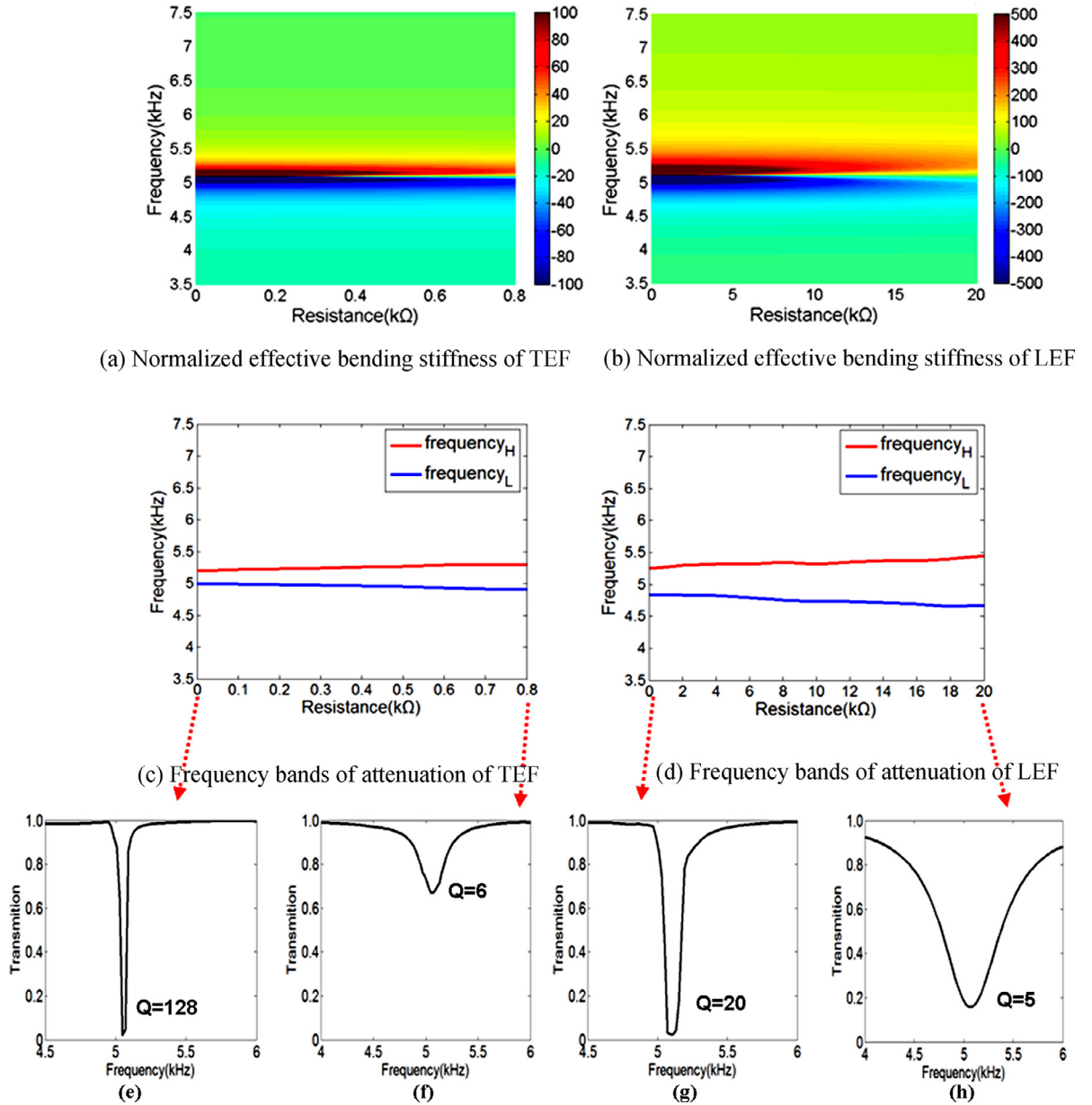
Fig. 6. Tuning characteristics of the TEF and LEF metamaterial beams with different resistance values. (a) and (b) Normalized effective bending stiffnesses (D_{eff}/D_b) as functions of both frequency and resistance value for TEF and LEF, respectively, where the unit of the normalized effective bending stiffnesses (D_{eff}/D_b) is 1. (c) and (d) Relationships between the frequency bands for bending wave attenuation and the resistance values based on the theoretical results of dispersion curves obtained by using Eq. (19) for TEF and LEF metamaterial beams, respectively. (e) and (f) Transmission curves obtained for the TEF metamaterial beam when $R=0$ and 0.8 kΩ, respectively. (g) and (h) Transmission curves obtained for the LEF metamaterial beam when $R=0$ and 20 kΩ, respectively.

As the R value increased from 0 to 20 kΩ, the Q factor changed from 20 to 5, and wave attenuation changed less (the transmission value changed little from 0.016 to 0.17).

It can be seen that the Q factor of the transmission curve for $R=20$ kΩ is not notably lower than that for $R=0$. Therefore, with an increased resistance value, the LEF metamaterial beam can still obtain good wave attenuation characteristics (a transmission of 0.17) when the bandgap is approximately twice that for $R=0$. For the TEF metamaterial beam, when the bandgap is approximately twice that for $R=0$, the wave attenuation characteristic becomes worse obviously (a transmission of 0.67). The main reason for this phenomenon is that the piezoelectric shunting of the LEF metamaterial beam is with stronger piezoelectric coupling, which results in its stronger vibration attenuation capability.
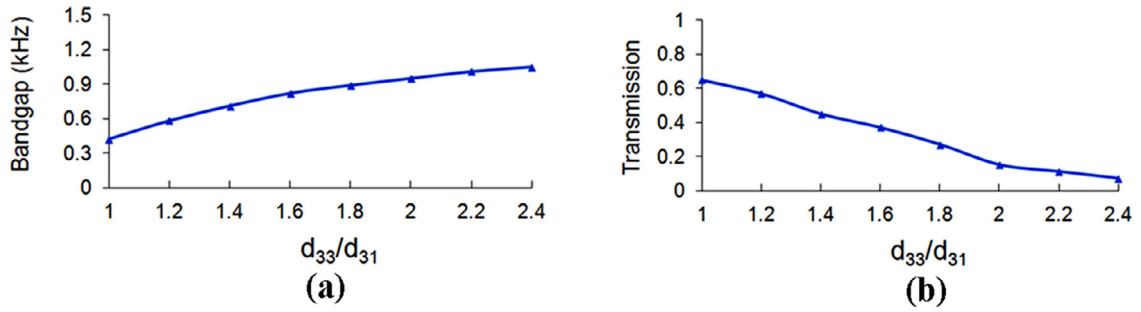
Fig. 7. Influences of the value of d_{33}/d_{31} on the (a) bandgap and (b) transmission for LEF metamaterial beams.
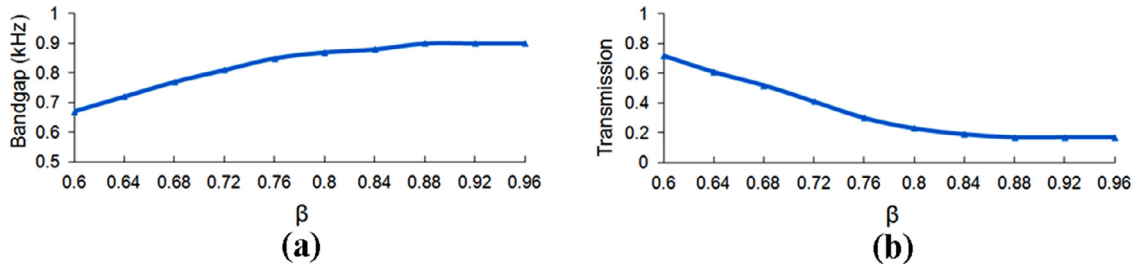

Fig. 8. Influences of the value of $\beta = l_p/l_b$ on the (a) bandgap and (b) transmission for LEF metamaterial beams.

To describe the influences of d_{33}/d_{31} on the vibration characteristics of LEF metamaterial beams, Fig. 7(a) shows the relationship between the bandgap and the value of d_{33}/d_{31}. Fig. 7(b) shows the relationship between the transmission and the value of d_{33}/d_{31}. In this case, $R = 20$ kΩ and $L_2 = 9025$ mH. In addition to d_{33}, the geometric and material parameters of the unit cells were set to those listed in Table 1. The figures show that, with increasing d_{33}/d_{31}, the bandgap becomes wider, while the transmission decreases; that is, the vibration attenuation depth becomes greater.

The influence of the length of the piezoelectric plate on the vibration characteristics of LEF metamaterial beams was also examined. $\beta = l_p/l_b$ was used to describe the relative length of the piezoelectric plate (where l_p is the length of the piezoelectric plate in the LEF unit cell, and l_b is the length of the metal beam in the LEF unit cell). In this case, $R = 20$ kΩ and $L_2 = 9025$ mH. In addition to the length of the piezoelectric plate, l_p, the geometric and material parameters of the unit cells were set to those listed in Table 1. Fig. 8(a) shows the relationship between the bandgap and the value of β, and Fig. 8(b) shows the relationship between the transmission and the value of β. The figures show that, with increasing β, the bandgap increases significantly, while the transmission decreases; that is, the vibration attenuation depth becomes greater. When the value of β is larger than 0.88, the bandgap and the transmission hardly change. This suggests that there exists a threshold value of β. To obtain good vibration attenuation characteristics, β must be larger than this threshold value. The main mechanism is that, with a larger relative length of the piezoelectric plate, the piezoelectric actuator can obtain stronger local resonances, and thus its regulating ability is more obvious. Consequently, better vibration attenuation characteristics can be obtained. When the relative length of the piezoelectric plate is sufficiently large, the regulating ability no longer increases obviously.

The resistance and inductance together create a complex electrical impedance for the resonant shunt. The combination of the inductance and the capacitance of the piezoelectric patch produces an electrical oscillator, which is similar to a mass–spring mechanical resonance unit generating a mechanical oscillation. For TEF resonators, when the resistance increases, the resonance strength decreases, and the resulting vibration attenuation capability is notably weakened. The vibration attenuation capability is closely related to the strength of the piezoelectric coupling of the resonators. Because LEF resonators exhibit stronger piezoelectric coupling and resonance capability, when resonance occurs, the extra transferred energy of LEF resonators compared with TEF resonators is reflected in the greater vibration attenuation depth when the increasing degree of the bandgap width of the two cases are similar. In other words, for LEF resonators, the stronger piezoelectric coupling induced that the decreasing degree of the resonance strength is lower than that of TEF resonators when the resistance increases. This phenomenon indicates that the mechanical vibration attenuation ability of LEF resonators is not significantly weakened by the increase in the resistance. Therefore, the proposed LEF metamaterial beam could maintain better vibration attenuation properties when the bandgap width is broadened by increasing the resistance value compared with the TEF metamaterial beam.

5. Conclusion

In this study, a piezoelectric unit cell with an LEF is proposed to improve the resistance-tuning characteristics of a metamaterial beam. The effective stiffness and bandgaps were calculated by a theoretical method and verified by numerical simulations. The results show that, compared with the traditional TEF metamaterial beam, the LEF metamaterial beam can obtain better resistance-tuning and vibration attenuation characteristics. LEF resonators have a stronger piezoelectric coupling compared to TEF resonators. As a result, the decreasing degree of the resonance strength is lower than that of the TEF resonators when the resistance increases. This phenomenon indicates that the mechanical vibration attenuation ability of LEF resonators is not significantly weakened by the increase in the resistance. Therefore, compared with the traditional TEF metamaterial beam, the proposed LEF metamaterial beam could maintain better vibration attenuation properties when the bandgap width is broadened by tuning the resistance value.

Declaration of Competing Interest

We declare that we have no known competing financial interest or personal relationships that could have appeared to influence the work reported in this paper.

CRediT authorship contribution statement

Tingfeng Ma: Conceptualization, Methodology, Supervision, Writing - original draft. **Yangyang Chen:** Data curation. **Hui Chen:** Data curation, Visualization. **Yuanzhen Zheng:** Visualization. **Guoliang Huang:** Supervision. **Ji Wang:** Validation. **Jianke Du:** Writing - review & editing.

Acknowledgements

References

[1] Y. Achaoui, A. Khelif, S. Benchabane, L. Robert, V. Laude, Experimental observation of locally-resonant and Bragg band gaps for surface guided waves in a phononic crystal of pillars, Phys. Rev. B 83 (2011) 104201.
[2] A.P. Liu, X.M. Zhou, G.L. Huang, G.K. Hu, Super-resolution imaging by resonant tunneling in anisotropic acoustic metamaterials, J. Acoust. Soc. Am. 132 (2012) 2800–2806.
[3] J.A. Monsoriu, R.A. Depine, M.L. Martínez-Ricci, E. Silvestre, Interaction between non-Bragg band gaps in 1D metamaterial photonic crystals, Opt. Express 14 (2006) 12958–12967.
[4] L. Liu, M.I. Hussein, Wave motion in periodic flexural beams and characterization of the transition between Bragg scattering and local resonance, ASME J. Appl. Mech. 79 (2012) 011003.
[5] Z. Liu, X. Zhang, Y. Mao, Y.Y. Zhu, Z. Yang, C.T. Chan, P. Sheng, Locally resonant sonic materials, Science 289 (2000) 1734–1736.
[6] K.T. Tan, H.H. Huang, C.T. Sun, Blast-wave impact mitigation using negative effective mass density concept of elastic metamaterials, Int. J. Impact Eng. 64 (2014) 20–29.
[7] D.L. Yu, Y.Z. Liu, G. Wang, H.G. Zhao, J. Qiu, Flexural vibration band gaps in Timoshenko beams with locally resonant structure, J. Appl. Phys. 100 (2006) 124901.
[8] M. Oudich, M.B. Assouar, Z.L. Hou, Propagation of acoustic waves and waveguiding in a two-dimensional locally resonant phononic crystal plate, Appl. Phys. Lett. 97 (2010) 193503.
[9] K. T. Tan, H. H. Huang, C. T. Sun, Negative effective mass density of acoustic metamaterial using dual-resonator spring-mass model, in: Metamaterials '2012: Proceeding of the sixth international congress on advanced electromagnetic materials in microwaves and optics, 2012, pp. 29–31.
[10] M. Nouh, O. Aldraihem, A. Baz, Wave propagation in metamaterial plates with periodic local resonances, J. Sound Vib 341 (2015) 53–57.
[11] L. Raghavan, A. Srikantha Phani, Local resonance bandgaps in periodic media: Theory and experiment, J. Acoust. Soc. Am. 134 (2013) 1950–1959.
[12] R. Zhu, X.N. Liu, G.K. Hu, C.T. Sun, G.L. Huang, A chiral elastic metamaterial beam for broadband vibration suppression, J. Sound Vib 333 (2014) 2759–2773.
[13] S.A. Pope, H. Laalej, S. Daley, Performance and stability analysis of active elastic metamaterials with a tunable double negative response, Smart Mater. Struct. 21 (2012) 125021.
[14] J.D. Hobeck, D.J. Inman, Magnetoelastic metastructures for passive broadband vibration suppression, in: Proceeding of SPIE, Active and Passive Smart Structures and Integrated Systems (2015) 943119.
[15] M. Nouh, O. Aldraihem, A. Baz, Wave propagation in metamaterial plates with periodic local resonances, J. Sound Vib 341 (2015) 53–73.
[16] N.W. Hagood, A. von Flotow, Damping of structural vibrations with piezoelectric materials and passive electrical networks, J. Sound Vib 146 (1991) 243–268.
[17] A.E. Bergamini, T. Delpero, L.D. Simoni, L.D. Lillo, M. Ruzzene, P. Ermanni, Phononic crystal with adaptive connectivity, Adv. Mater. 9 (2014) 1343–1347.
[18] C. Sugino, S. Leadenham, M. Ruzzene1, A. Erturk, An investigation of electroelastic bandgap formation in locally resonant piezoelectric metastructures, Smart Mater. Struct. 25 (2017) 105036.
[19] F. Casadei, T. Delpero, A. Bergamini, P. Ermanni, M. Ruzzene, Piezoelectric resonator arrays for tunable acoustic waveguides and metamaterials, J. Appl. Phys. 112 (2012) 064902.
[20] Y.Y. Chen, G.K. Hu, G.L. Huang, A hybrid elastic metamaterial with negative mass density and tunable bending stiffness, J. Mech. Phys. Solids 105 (2017) 179–198.
[21] W.L. Zhou, Y. Wu, L. Zuo, Vibration and wave propagation attenuation for metamaterials by periodic piezoelectric arrays with high-order resonant circuit shunts, Smart Mater. Struct. 24 (2015) 065021.
[22] N. Kherraz, L. Haumesser, F. Levassort, P. Benard, B. Morvan, Hybridization bandgap induced by an electrical resonance in piezoelectric metamaterial plates, J. Appl. Phys. 123 (2018) 094901.

[23] S.L. Li, J.W. Xu, J. Tang, Adaptive acoustic metamaterial with periodic piezoelectric network, in: Proc. SPIE 10164, Active and passive smart structures and integrated systems, 2017.

[24] W. Zhou, W.Chen Muhammad, Z. Chen, C.W. Lim, Actively controllable flexural wave band gaps in beam-type acoustic metamaterials with shunted piezoelectric patches, Eur. J. Mech A-Solid 77 (2019) 103807.

[25] Y. Jin, B. Bonello, Y. Pan, Acoustic metamaterials with piezoelectric resonant structures, J. Phys. D: Appl. Phys. 47 (2014) 245301.

[26] Z. Chen, C. Xue, L. Fan, S.Y. Zhang, X.J. Li, H. Zhang, J. Ding, A tunable acoustic metamaterial with double-negativity driven by electromagnets, Sci. Rep. 6 (2016) 30254.

[27] L. Airoldi, M. Ruzzene, Design of tunable acoustic metamaterials through periodic arrays of resonant shunted piezos, New J. Phys. 13 (2011) 113010.

[28] T. Delpero, in: Design of adaptive structures with piezoelectric materials (Doctoral Thesis), Swiss Federal Institute of Technology Zurich, Zurich, 2014.

[29] V. D. Kugel, S. Chandran, and L. E. Cross, Caterpillar-type piezoelectric d bimorph transducer, Appl. Phys. Lett. 69(1996) 2021.

[30] J. Kahn, Acoustic and elastic properties of PZT ceramics with anisotropic pores, J. Am. Ceram. Soc. 68 (1985) 623–628.